Transcranial electrical stimulation effects on neurovascular coupling

Yashika Arora
NBRC, India
Anirban Dutta (anirband@buffalo.edu)
University at Buffalo

Short Report

Keywords: tDCS, tES, neurovascular coupling, fNIRS, fMRI

Posted Date: March 9th, 2022

DOI: https://doi.org/10.21203/rs.3.rs-1429599/v1

Transcranial electrical stimulation effects on neurovascular coupling

Yashika Arora[1], and Anirban Dutta[2]
1. National Brain Research Centre, Manesar, India
2. Department of Biomedical Engineering, University at Buffalo, Buffalo, USA

Abstract

Transcranial electrical stimulation (tES) can exert cerebrovascular effects, but the mechanisms are unclear. Long-term (≥3min) transcranial direct current stimulation (tDCS) can also change the extracellular ion concentrations that can modulate neuronal excitability. An increase in interstitial K+ can modulate the neurovascular system's sensitivity via Kir channels in the astrocytes and the mural cells.

To gain a mechanistic understanding of the tES effects on neurovascular coupling (NVC), we used a physiologically constrained multi-compartmental model (having nested pathways) for modal analysis to study the dynamic properties of the system for the output changes in blood vessel circumference and their natural frequencies in the frequency domain. Then, we used the open-source rsHRF toolbox and the functional magnetic resonance imaging (fMRI)-tDCS dataset to show the effects of anodal tDCS on hemodynamic response function (HRF) in the grey matter and at three regions of interest in the grey matter underlying anodal electrode (FC5), cathodal electrode (FP2), and an independent site remote from the electrodes (PZ). A canonical HRF model and a Finite Impulse Response (FIR) model captured the anodal tDCS effects on the temporal profile of the HRF. The modal analysis characterized the tES's vascular effects through neuronal and non-neuronal pathways, where stable modes were found for the smooth muscle cell compartment in the 0Hz-0.05Hz range.

Our study showed tDCS onset effects on the neurovascular coupling (and HRF) for verum and sham tDCS conditions that were different from the no tDCS condition, which questions the validity of the placebo. Therefore, it is crucial to avoid fitting a common HRF for the whole brain, and disentangling the tES effect on the HRF is critical to the fMRI-tES studies. Future studies also need to address the trade-off between bias (in canonical HRF) and variance (in FIR HRF) that can be achieved by applying a mechanistic grey-box model.

1 Introduction

Ekhtiari and colleagues [1] recently published a checklist for assessing the methodological quality of concurrent transcranial electrical stimulation (tES)-functional magnetic resonance imaging (fMRI) studies; however, the protocol did not elaborate on the methods for separating tES effect on the neuronal activation from the effect on the neurovascular coupling [2], i.e., the hemodynamic response function (HRF). Here, mapping of the tES stimulus-related Blood Oxygen Level Dependent (BOLD) signals measured using fMRI is usually achieved by fitting a general linear model (GLM) to the time course with a pre-specified canonical HRF model, e.g., double-gamma function [3]. Such a canonical HRF univariate model [3] with a single dilation parameter limits physiological interpretability of the neurovascular coupling, which is crucial since tES has been shown to affect the neurovascular coupling in health [4] and disease [5] based on the electric field distribution [2].

Spatial localization of HRF has been proposed by Vincent et al. [6] that addresses HRF recovery and localization of the cerebral activity using a black-box Finite Impulse Response (FIR) and temporally regularized FIR models. Yashika et al. [2] published a biophysically informed neurovascular coupling model to capture the hemodynamic response to tES based on functional near-infrared spectroscopy (fNIRS). Yashika et al. [2] addressed the challenge to find a trade-off between estimation bias and overfitting to fNIRS data by reducing the degrees of freedom in a grey-box model. Grey-box modeling can also be applied to BOLD data for HRF recovery, e.g., one HRF per voxel, which can be used on either volume-based data sets or on data projected onto the cortical surface to reduce the computational needs for inference [6]. Here, the solution with the best fit to the electric field distribution, i.e., the source signal, can be selected using a cost function with regularization in the tES-fMRI studies.

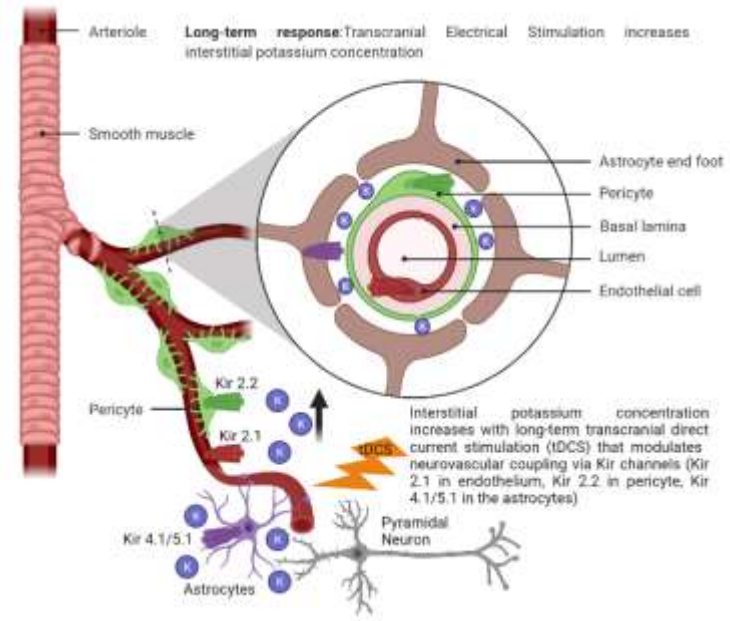

Figure 1: (a) Long-term (≥3min) transcranial electrical stimulation can change the interstitial concentration of potassium that will modulate the neurovascular system's sensitivity via Kir channels. (b) Four compartment lumped physiological model of the neurovascular unit that can be perturbed by the tES current density leading to vessel response in terms of diameter changes.

Various tES modalities have differences in the temporal profile of the current stimulation. In transcranial direct current stimulation (tDCS), the current profile has a monophasic, non-oscillating constant value. In contrast, in transcranial alternating current stimulation (tACS), the oscillating current reverses the flow rhythmically at a specific frequency. For example, tACS differs from tDCS in that it provides a mechanism for manipulating intrinsic oscillations through the injection of sinusoidal currents [8-10]. Then, the other methods are transcranial oscillating current stimulation (tOCS) which uses tDCS to set a baseline to the tACS oscillations, and transcranial random noise stimulation (tRNS)

that injects 'noisy' current with bounded stochasticity [7, 8]. Because tES's modulatory effects on blood vessels can be mediated by the neuronal and non-neuronal cells in the neurovascular tissue, a deeper understanding of the signalling pathways will be crucial for a mechanistic understanding of the effects of tES, including entrainment effects [7].

In this paper, we applied a computational modeling approach [11] based on the physiology of the neurovascular tissues for assessing the vascular response to electric fields generated by tES through various pathways in the neurovascular unit (NVU), as shown in Figure 1. The physiological model considered the lumped neurovascular system of vascular smooth muscle (SMC) space, perivascular space, synaptic space, and the astrocyte space; and captured the tES induced direct and indirect vascular responses. Here, modal analysis can provide the characteristic dynamics of a system from its natural frequencies, mode shapes, and damping factors and develop a mathematical model of the system's behavior. Typically, this method is prevalently used in structural and fluid mechanics and can be well applied for biomedical system analysis to derive the modal behavior of the output responses [12, 13]. The detailed physiological NVU model [11] has been shown to simulate vessel oscillations in the range of 0.05–0.2 Hz governed by the interactions between the Kir 2.1 channels on the endothelium and the Kir 2.2 channels on the pericytes [8],[9]. In this study, we used the modal analysis approach to analyze the physiologically detailed NVU model for evaluating neurovascular coupling modes that may be perturbed with tACS. We also used a nonparametric impulse response estimation of the HRF from an open-source fMRI-tDCS dataset [10] and compared that with the canonical HRF to elucidate tES effects on the temporal profile of the HRF.

2 Material and Methods

2.1 Physiological modeling

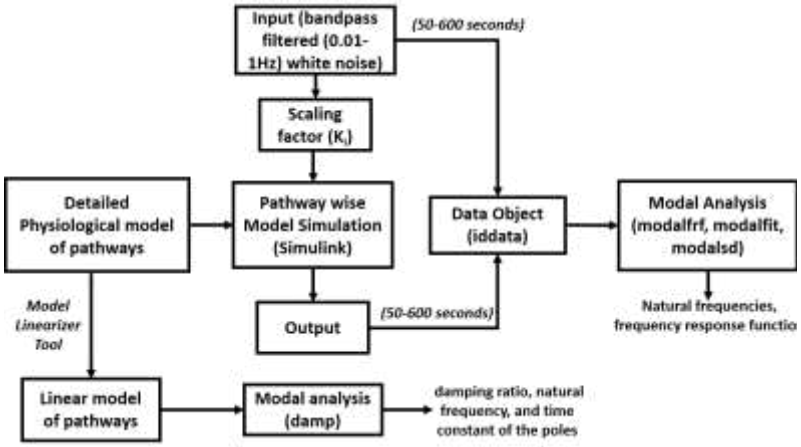

Figure 2: Modal analysis approach used for evaluating the physiological model using Matlab and Simulink (Mathworks Inc., USA).

To comprehend the mechanistic aspects of tES techniques, we used a mathematical model [11] based on neurovascular tissue physiology to evaluate the vascular response through various pathways that are susceptible to the electric fields generated by tES as shown in Figure 1. The simulation model included four compartments based on published literature where the tES current density perturbed synaptic potassium released from active neurons for the Pathway 1, astrocytic transmembrane current for the Pathway 2, perivascular potassium concentration for the Pathway 3, and voltage-gated ion channel current on the SMC for the Pathway 4. The implementation of the model is presented in Yashika et al. [11]. The physiologically detailed models were simulated using the 'ode23tb' solver in Simulink (MathWorks, Inc., USA). Prior work showed that the models simulated oscillations in the range of 0.05-0.2 Hz generated by interactions between the potassium dynamics and the calcium dynamics in the perivascular space [8].

2.2 Modal analysis

Figure 2 shows the block diagram of the modal analysis work flow using Matlab and Simulink packages (Mathworks, Inc., USA). For modal analysis, we applied ten tES perturbations which were bandpass filtered

(0.01-1 Hz) white noise inputs of 600 seconds to the four physiologically constrained NVU pathways shown in Figure 2a (equations are presented in the supplementary materials from Yashika et al. [11]). The input and output time series were stored using a time-domain data object ('iddata' in MATLAB, MathWorks, Inc., USA). We excluded the initial 50 seconds of the transient response in the time series data for modal analysis. We used modal analysis functions: 'modalfrf' to determine frequency-response functions for modal analysis, 'modalfit' to determine modal parameters from the frequency-response functions, and 'modalsd' to generate a stabilization diagram for modal analysis on the data object in Matlab (MathWorks, Inc., USA). First, the frequency response functions for the four tES pathways of the NVU system were found using 'modalfrf' for a sample rate of 10 samples per second (10 Hz), where the noise was assumed to be uncorrelated with the input signals. Then, the natural frequencies of the four tES pathways for the NVU system were found from the frequency-response using the 'peak-picking' method (a fast and straightforward procedure for identifying peaks in the frequency response functions) available in the 'modalfit' function in the physiological frequency range of 0.01-0.2 Hz. Then, a single set of modal parameters were generated using the least-squares complex exponential (LSCE) algorithm by analyzing multiple response signals simultaneously in 'modalsd.' Here, a stabilization diagram is used to identify the physical modes by examining the stability of poles as the number of modes increases. Then, the linear model of the four physiologically detailed tES pathways in the NVU was found using the Model Linearizer tool in the Simulink (MathWorks, Inc., USA) linear analysis package. The damping ratio, natural frequency, and the time constant of the poles were obtained using the 'damp' function from the linear model system.

2.3 fNIRS-tDCS and fMRI-tDCS HRF fitting

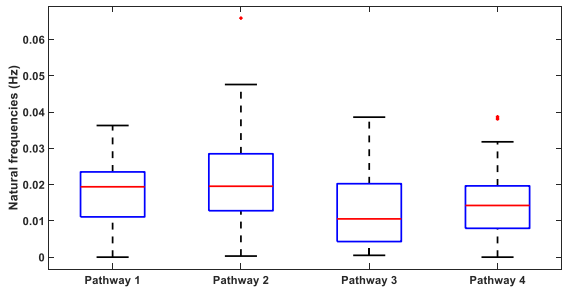

Figure 3: Boxplot of the natural frequencies obtained through modal analysis for the four tES perturbation model pathways. On each box, the central mark indicates the median, and the bottom and top edges of the box indicate the 25th and 75th percentiles, respectively. The whiskers extend to the most extreme data points not considered outliers, and the outliers are plotted individually using the red '+' symbol.

Yashika et al. [11] presented the minimal realization transfer functions for the four pathways (see Figure 1b) based on the fNIRS-tDCS dataset at TR = 3.36 sec [10] that provided a qualitative analysis of the hemodynamic response where the tDCS perturbation Pathway 4 had the fastest response (peaked at 0.4 sec), and the tDCS perturbation Pathway 1 had the slowest response (peaked at 5 sec). Grey-box modeling by Yashika et al. [11] was based on prior works using fNIRS [11] and fNIRS in conjunction with electroencephalography (EEG) [4] that postulated [8] tES led increase in interstitial K+ that can modulate the neurovascular system's sensitivity via Kir channels [12] (see Figure 1), and the interaction with the calcium activity in the capillary pericytes [8],[9]. In this study, we used an open-source tES-fMRI dataset [10] that showed no field inhomogeneity in functional sensitivity metrics in the grey matter during 2mA anodal tDCS that was delivered for 20 mins to the frontal cortex (anode at FC5 and cathode at FP2 in a 10-20 system). Also, the fMRI data were collected during sham-tDCS and no-tDCS conditions. Here, sham-tDCS is postulated to evoke an onset response (discussed in detail by Yashika et al. [11]); however, the no-tDCS condition should not have any onset response. We used canonical HRF with time & dispersion derivatives and an FIR model in the rsHRF toolbox [13] to elucidate the tDCS onset effects on the temporal profile of the HRF. The FIR model was found using a nonparametric impulse response estimation ('impulseest' in Matlab, Mathworks, Inc., USA). The HRF estimation was performed using the rsHRF toolbox [13] that elucidated the effects of anodal tDCS on HRF in the grey matter as well as at the three regions of interest (ROIs) in the grey matter underlying anodal electrode (FC5), cathodal electrode (FP2), and an independent site remote from the electrodes (PZ).

3 Results

Table 1 lists the natural frequencies obtained using the 'peak-picking' algorithm following the modal analysis of the physiologically detailed non-linear model of the four tES perturbation pathways using ten different seeds for the white Gaussian noise. The 'peak-picking' method is a local single-degree-of-freedom method where the peaks for each mode are considered independently. Here. The natural frequencies across all the four tES perturbation pathways were less than ~0.05 Hz – see Figure 3. Figure 3 depicts the boxplot of these natural frequencies within 0.01-0.2Hz across ten different runs (with different seed – see Table 1) of the modal analysis for the four tES perturbation pathways, Pathway 1: tES perturbing vessel response through synaptic potassium pathway, Pathway 2: tES perturbing vessel response through the astrocytic pathway, Pathway 3: tES perturbing vessel response through perivascular potassium pathway, and Pathway 4: tES perturbing vessel response through the SMC pathway. We also applied a global multiple-degree-of-freedom method, LSCE, where the parameters for all modes were estimated simultaneously from multiple frequency-response functions. Figure 4 shows the stabilization diagrams and output of the natural frequencies of the poles, which were stable in frequency. We observed many stable modes in the 0.01-0.05 Hz (see Figure 3) frequency range mainly in the tES perturbation Pathway 4 where that pathway is related to SMC compartment of the NVU. The poles and the damping parameters associated with the linearized models of the four tES perturbation pathways are listed in Table S1 in the supplementary materials.

Table 1: Natural frequencies obtained from the modal analysis (workflow block diagram in Figure 2) of the four physiologically detailed tES perturbation pathways

Pathways in columns and different runs with different seeds for the bandpass filtered white noise input in the rows	Pathway 1	Pathway 2	Pathway 3	Pathway 4
Run 1	0.0000, 0.0193	0.0247	0.0052, 0.0157, 0.0265	0.0000, 0.0069, 0.0201
Run 2	0.0189, 0.0201	0.0003, 0.0156, 0.0167	0.0025, 0.0231, 0.0235	0.0128, 0.0141,
Run 3	0.0000, 0.0153, 0.0195	0.0109, 0.0191, 0.0288, 0.0476	0.0027, 0.0081, 0.0196, 0.0236	0.0067, 0.0090, 0.0144
Run 4	0.0115, 0.0245	NaN	0.0050	0.0020, 0.0168
Run 5	0.0007, 0.0077, 0.0200, 0.0276	0.0131	0.0005, 0.0128, 0.0176	0.0192, 0.0318
Run 6	0.0179, 0.0363	0.0237, 0.0418	0.0055	0.0104, 0.0171
Run 7	0.0107, 0.0131	0.0128, 0.0200, 0.0380, 0.0659	0.0036 0.0386	0.0381
Run 8	0.0225, 0.0298	0.0048, 0.0100	0.0011, 0.0209	0.0043, 0.0223
Run 9	0.0000, 0.0215	0.0038, 0.0285	0.0033, 0.0083, 0.0184	0.0099, 0.0164
Run 10	0.0198, 0.0319, 0.0360	0.0189, 0.0229, 0.0242	0.0058, 0.0188	0.0387

Figure S1 in the supplementary materials show the electrical field distribution for 2mA tDCS with FC5 (anodal electrode) and FP2 (cathodal electrode) computed with the ROAST package [14] for the open-source tES-fMRI dataset [10]. Figure 5(a) shows the functional sensitivity metrics calculated using the open-source code and data from the tES-fMRI dataset [10], where anodal tDCS (figure legend: anodal) led to a shift to a higher t-score (first row of Figure 5(a)). Here, the No-tDCS and the Sham-tDCS conditions resulted in a similar HRF temporal profile different from the anodal tDCS condition based on the canonical HRF model. At the same time, the width of the frequency distributions (second row of Figure 5(a)) remained similar across conditions (figure legends: Sham for sham-tDCS, No for no-tDCS conditions), reflecting similar field inhomogeneity.

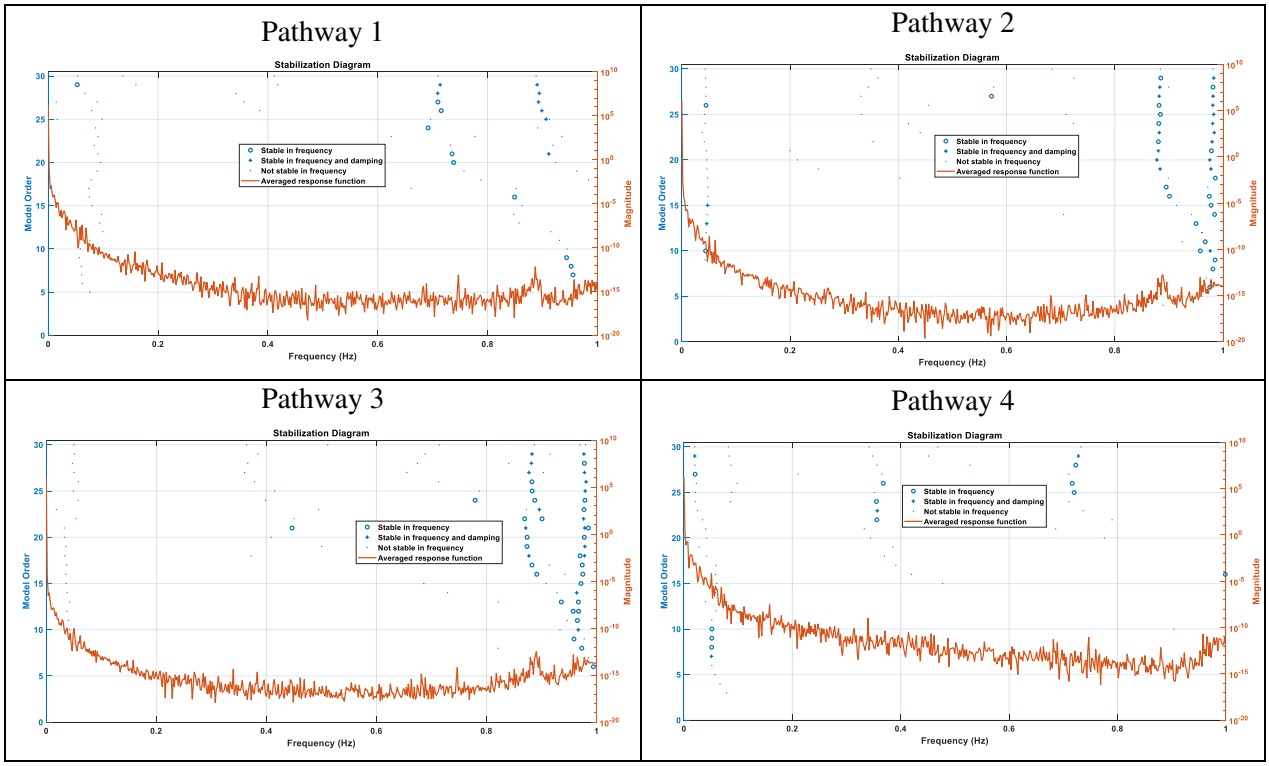

Figure 4: Stabilization diagrams obtained for the four tES perturbation pathways

We also applied HRF estimation using the rsHRF toolbox[13] that elucidated the effects of anodal tDCS at four ROIs in the grey matter. Figure 5(b) shows that the canonical HRF with time & dispersion derivatives primarily captured the tES effects on the magnitude of the main response and the magnitude of undershoot. In contrast, the FIR model captured the impact on the whole temporal profile of the HRF. Here, we observed that both the anodal tDCS condition and sham tDCS condition had similar FIR at the FC5 (anodal electrode) and PZ (remote location) ROIs based on the nonparametric impulse response estimation that captured the onset response to tDCS in both the conditions which was found to be different from the no-tDCS condition. For the FP2 (cathodal electrode) ROI, the FIR-based HRFs differed across all conditions, specifically anodal tDCS and sham tDCS conditions. Figure 6 shows an estimation of the probability density function across all the voxels for the height parameter of the HRF found using the open-source rsHRF toolbox [13]. The No-tDCS condition shown with red color resulted in a higher expectation of a lower height HRF parameter than the Sham-tDCS (green color) and the Anodal-tDCS (blue color) conditions from canonical HRF with time & dispersion derivatives as well as finite impulse response model. Here, the Sham-tDCS

(green color) and the Anodal-tDCS (blue color) conditions shifted the expectation toward a higher HRF height parameter.

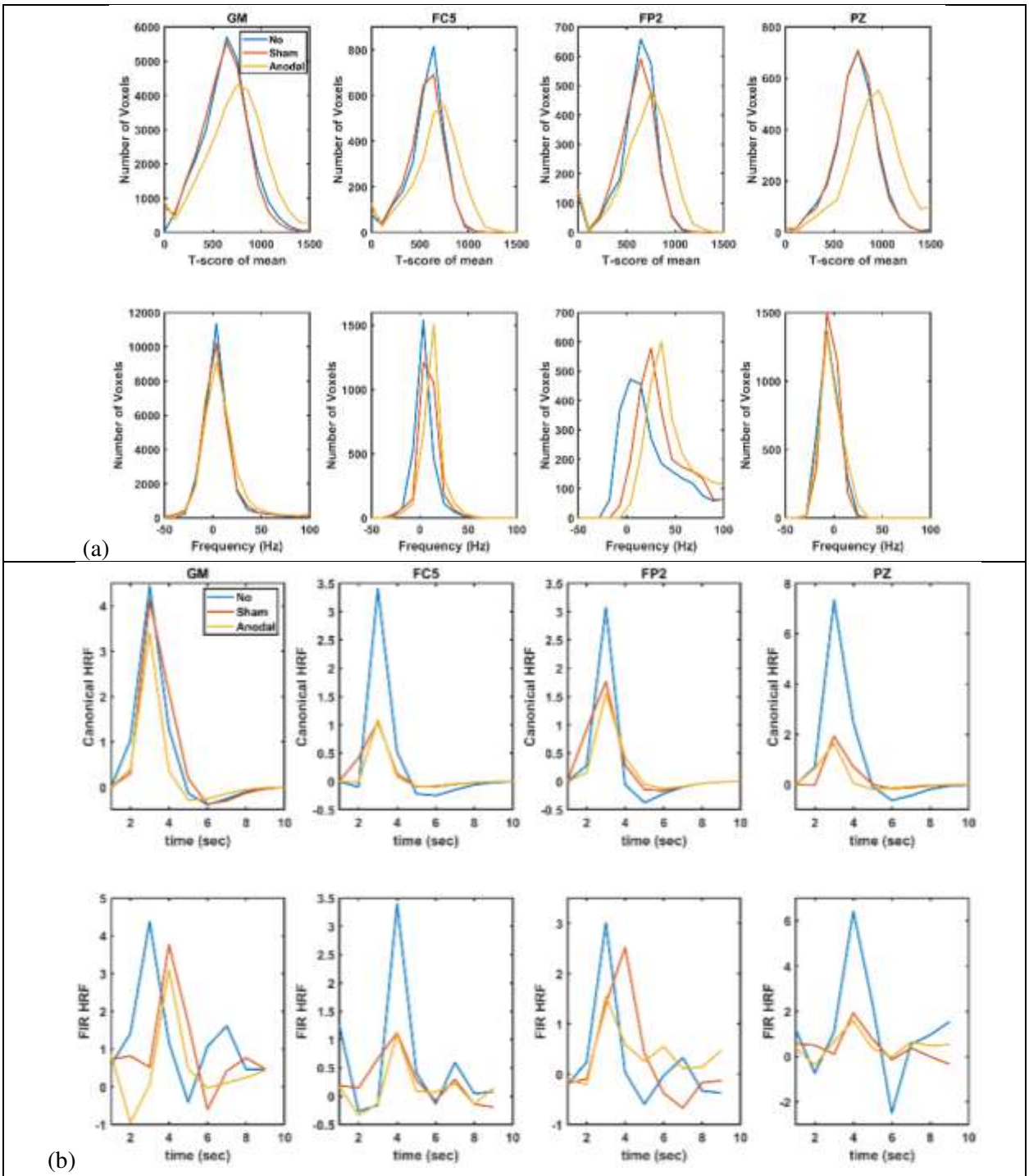

Figure 5: (a) Functional sensitivity metrics: top row shows the t-score of the mean in the grey matter (GM) and the grey matter ROIs, FC5 (anodal electrode), FP2 (cathodal electrode), PZ (remote location) while the bottom row shows the corresponding offset frequency (in Hz) to capture field inhomogeneity. (b) Estimated hemodynamic response function (HRF) in the grey matter (GM) and the grey matter ROIs, FC5 (anodal electrode), FP2 (cathodal electrode), PZ (remote location) where the top row shows the

results using canonical HRF with time & dispersion derivatives while the bottom row shows the results using a finite impulse response (FIR) model. Figure legends: No means no-tDCS condition, Sham means Sham-tDCS condition, Anodal means Anodal-tDCS condition.

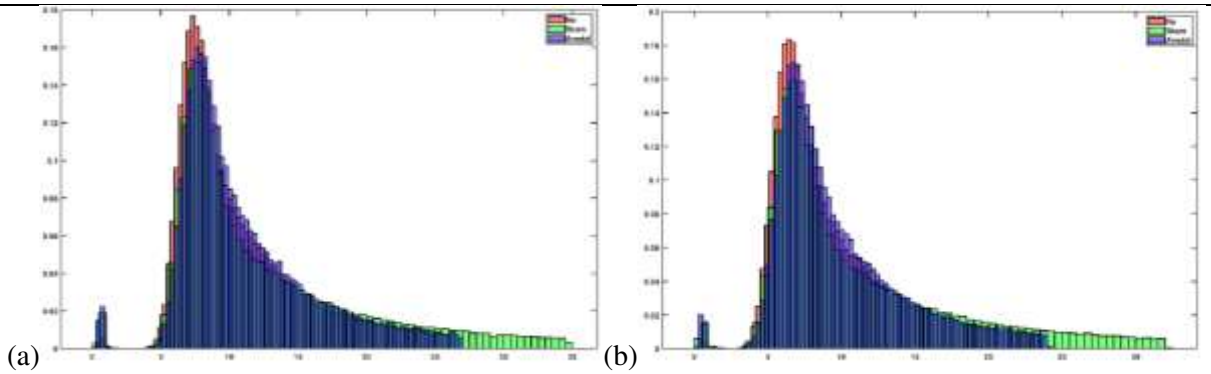

(a) (b)

Figure 6: (a) An estimation of the probability density function across all the voxels for the height parameter (in the x-axis) of the HRF using canonical HRF with time & dispersion derivatives. (b) An estimation of the probability density function across all the voxels for the height parameter (in the x-axis) of the HRF using finite impulse response model.

4 Discussion

Our study provided a mechanistic understanding of the four physiologically detailed tES pathways in the NVU in terms of their frequency-response functions, which can be leveraged for optimizing tES parameters, including the frequency [7]. Specifically, many stable modes were found to be in the 0 Hz to 0.05 Hz range in tES Pathway 4 which may be leveraged to develop tES therapeutic measures: vascular factors contribute to cerebrovascular disease and mild cognitive impairment and dementia [15], which are predicted to affect 152 million people by 2050 (Alzheimer's Disease International London, UK, 2019). Various physiologically relevant frequency bands have already been identified in the literature: 0.6–2 Hz and 0.145–0.6 Hz are related to cardiac and respiratory function, respectively, 0.052–0.145 Hz is associated with smooth muscle cell activity, and 0.021–0.052 Hz may reflect smooth muscle cell autonomic innervation [16]. Within the frequency range of 0.1 Hz to 10 Hz, Yashika et al. [7] found that the vessel oscillations were more sensitive to tOCS than to the tACS, and entrainment effects were more pronounced for lower frequencies. Here, Kir 2.1 channels on the endothelium and Kir 2.2 channels on the pericytes can modulate [8],[9] the neurovascular coupling underlying HRF, as shown in Figure 1(a), which may have a therapeutic potential in aging and Alzheimer's disease [17]. Therefore, tES modulation of neurovascular coupling and its role in

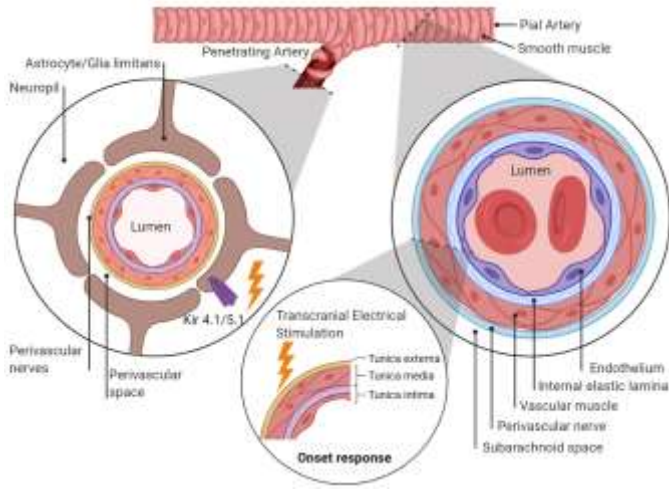

Figure 7: Short-term (<3min) transcranial electrical stimulation can lead to an onset response via perivascular nerves. Also, Kir 4.1/5.1 channels in the astrocytes can play a role in the perivascular space.

facilitating neural processing is crucial [18]. Since we found stable modes in the 0 Hz to 0.05 Hz range in tES Pathway 4 with the Nyquist frequency at 0.1Hz and a maximum TR=10sec for the fMRI-tDCS studies. The open-source fMRI-tDCS dataset [10] used in the current study had a TR=3.36sec so it also captured 0.052–0.145 Hz activity associated with smooth muscle cell activity.

An immediate vascular response to tDCS via the perivascular pathway has been postulated [2], where the interaction between the perivascular potassium and calcium concentration can lead to standalone steady-state vessel oscillations <0.1Hz found from computational modeling. Neuronal oscillations can entrain these vessel oscillations due to the shared extracellular space, and the neurovascular coupling can be investigated using joint imaging with fNIRS-EEG [8]. This provides a portable neuroimaging approach amenable to a point-of-care setting when compared to the fMRI-tES setup. Prior works [4],[5],[19] have found that long-term tDCS can change the neurovascular coupling status, which may be mediated by the Kir potassium channels in the mural cells [8], thereby changing the neurovascular system's sensitivity leading to aftereffects. However, short-term (<150sec) tDCS can also affect the hemodynamic response [2] that can be used for immediate control of hemodynamics using reduced dimension model predictive control (MPC). MPC uses an internal model for making predictions of the system behavior, considering the dynamics over a predefined prediction horizon, for optimizing the control actions. For online operation, MPC operates in a receding horizon fashion, i.e., new system measurements and new predictions into the future are made at each time step. Here, MPC can be based on minimal realization transfer functions for the four nested pathways for NVU [11], where tES current density (input pulse) can perturb a state variable at each of the four NVU compartments to perturb the vessel volume response (output).

This study found based on fMRI-tDCS dataset [10] that both the anodal tDCS condition and sham tDCS condition had similar FIR at the FC5 (anodal electrode) and PZ (remote location) ROIs based on the nonparametric impulse response estimation. Then, for the FP2 (cathodal electrode) ROI, the FIR based HRFs were different across all conditions, specifically anodal tDCS and sham tDCS conditions, which may be related to the modulation of local cortical inhibitory circuits and its interaction with the stimulation of the perivascular nerves and astrocytes (discussed in Yashika et al. [11] and shown in Figure 7). Figure 7 shows the proposed mechanism where the tDCS onset may directly stimulate the perivascular nerves and can also directly affect the astrocytes, as shown in Figure 1b, and directly affect the electrical communication in the arterial wall [20]. Here, onset response in the case of short-duration sham tDCS may explain the hidden source of variability [21]. Significantly, short-duration (< 3min) tDCS can have physiological effects in terms of onset response that has been discussed by Yashika et al. [2], where the biological effects can extend beyond the intended transient sensations [21]. However, a mechanistic understanding will require physiologically detailed modeling, invasive animal studies, and systems biology approaches [2]. Future invasive animal studies need to investigate the plasticity of the modulation of the mural cells [22] by long-term tES for the mechanistic understanding of the tES effects on neurovascular coupling.

Limitation of the current work includes unavailability of the fMRI-EEG data to capture the long-term effects of tES on the neurovascular coupling, as shown in Figure 1(a), where fNIRS-EEG has been shown feasible by computational modeling [4],[2]. Also, the trade-off between bias (in canonical HRF) and variance (in FIR HRF) achieved by applying mechanistic grey-box modeling of the NVU pathways [11] was not demonstrated, which is our future work.

5 References:

1. Ekhtiari, H., Ghobadi-Azbari, P., Thielscher, A., Antal, A., Li, L.M., Shereen, A.D., Cabral-Calderin, Y., Keeser, D., Bergmann, T.O., Jamil, A., Violante, I.R., Almeida, J., Meinzer, M., Siebner, H.R., Woods, A.J., Stagg, C.J., Abend, R., Antonenko, D., Auer, T., Bächinger, M., Baeken, C., Barron, H.C., Chase, H.W., Crinion, J., Datta, A., Davis, M.H., Ebrahimi, M., Esmaeilpour, Z., Falcone, B., Fiori, V., Ghodratitoostani, I., Gilam, G., Grabner, R.H., Greenspan, J.D., Groen, G., Hartwigsen, G., Hauser, T.U., Herrmann, C.S., Juan, C.-H., Krekelberg, B., Lefebvre, S., Liew, S.-L., Madsen, K.H., Mahdavifar-Khayati, R., Malmir, N., Marangolo, P., Martin, A.K., Meeker, T.J., Ardabili, H.M., Moisa, M., Momi, D., Mulyana, B., Opitz, A., Orlov, N., Ragert, P., Ruff, C.C., Ruffini, G., Ruttorf, M., Sangchooli, A., Schellhorn, K., Schlaug, G., Sehm, B., Soleimani, G., Tavakoli, H., Thompson, B., Timmann, D., Tsuchiyagaito, A., Ulrich, M., Vosskuhl, J., Weinrich, C.A., Zare-Bidoky, M., Zhang, X., Zoefel, B., Nitsche, M.A., Bikson, M.: A checklist for assessing the methodological quality of concurrent tES-fMRI studies (ContES checklist): a consensus study and statement. Nat Protoc. 1–24 (2022). https://doi.org/10.1038/s41596-021-00664-5.
2. Arora, Y., Walia, P., Hayashibe, M., Muthalib, M., Chowdhury, S.R., Perrey, S., Dutta, A.: Grey-box modeling and hypothesis testing of functional near-infrared spectroscopy-based cerebrovascular reactivity to anodal high-definition tDCS in healthy humans, https://www.researchsquare.com/article/rs-83907/v3, (2021). https://doi.org/10.21203/rs.3.rs-83907/v3.
3. Friston, K.J., Fletcher, P., Josephs, O., Holmes, A., Rugg, M.D., Turner, R.: Event-related fMRI: characterizing differential responses. Neuroimage. 7, 30–40 (1998). https://doi.org/10.1006/nimg.1997.0306.
4. Sood, M., Besson, P., Muthalib, M., Jindal, U., Perrey, S., Dutta, A., Hayashibe, M.: NIRS-EEG joint imaging during transcranial direct current stimulation: Online parameter estimation with an autoregressive model. J. Neurosci. Methods. 274, 71–80 (2016). https://doi.org/10.1016/j.jneumeth.2016.09.008.
5. Dutta, A., Jacob, A., Chowdhury, S.R., Das, A., Nitsche, M.A.: EEG-NIRS based assessment of neurovascular coupling during anodal transcranial direct current stimulation--a stroke case series. J Med Syst. 39, 205 (2015). https://doi.org/10.1007/s10916-015-0205-7.
6. Vincent, T., Badillo, S., Risser, L., Chaari, L., Bakhous, C., Forbes, F., Ciuciu, P.: Flexible multivariate hemodynamics fMRI data analyses and simulations with PyHRF. Front Neurosci. 8, 67 (2014). https://doi.org/10.3389/fnins.2014.00067.
7. Arora, Y., Chowdhury, S.R., Dutta, A.: Physiological neurovascular modeling of cerebrovascular effects of transcranial electrical current stimulation. Brain Stimulation: Basic, Translational, and Clinical Research in Neuromodulation. 14, 1597–1598 (2021). https://doi.org/10.1016/j.brs.2021.10.031.
8. Dutta, A.: Simultaneous functional near-infrared spectroscopy (fNIRS) and electroencephalogram (EEG) to elucidate neurovascular modulation by transcranial electrical stimulation (tES). Brain Stimul. 14, 1093–1094 (2021). https://doi.org/10.1016/j.brs.2021.07.019.
9. Glück, C., Ferrari, K.D., Binini, N., Keller, A., Saab, A.S., Stobart, J.L., Weber, B.: Distinct signatures of calcium activity in brain mural cells. eLife. 10, e70591 (2021). https://doi.org/10.7554/eLife.70591.
10. Nardo, D., Creasey, M., Negus, C., Pappa, K., Reid, A., Josephs, O., Callaghan, M.F., Crinion, J.T.: Transcranial direct current stimulation with functional magnetic resonance imaging: a detailed validation and operational guide, https://wellcomeopenresearch.org/articles/6-143, (2021). https://doi.org/10.12688/wellcomeopenres.16679.1.
11. Muthalib, M., Besson, P., Rothwell, J., Ward, T., Perrey, S.: Effects of Anodal High-Definition Transcranial Direct Current Stimulation on Bilateral Sensorimotor Cortex Activation During Sequential Finger Movements: An fNIRS Study. Adv Exp Med Biol. 876, 351–359 (2016). https://doi.org/10.1007/978-1-4939-3023-4_44.

12. Moshkforoush, A., Ashenagar, B., Harraz, O.F., Dabertrand, F., Longden, T.A., Nelson, M.T., Tsoukias, N.M.: The capillary Kir channel as sensor and amplifier of neuronal signals: Modeling insights on K+-mediated neurovascular communication. PNAS. 117, 16626–16637 (2020). https://doi.org/10.1073/pnas.2000151117.
13. Wu, G.-R., Colenbier, N., Van Den Bossche, S., Clauw, K., Johri, A., Tandon, M., Marinazzo, D.: rsHRF: A toolbox for resting-state HRF estimation and deconvolution. NeuroImage. 244, 118591 (2021). https://doi.org/10.1016/j.neuroimage.2021.118591.
14. Huang, Y., Datta, A., Bikson, M., Parra, L.C.: Realistic volumetric-approach to simulate transcranial electric stimulation—ROAST—a fully automated open-source pipeline. J. Neural Eng. 16, 056006 (2019). https://doi.org/10.1088/1741-2552/ab208d.
15. Pan, Y., Li, H., Wardlaw, J.M., Wang, Y.: A new dawn of preventing dementia by preventing cerebrovascular diseases. BMJ. 371, m3692 (2020). https://doi.org/10.1136/bmj.m3692.
16. Stefanovska, A., Bracic, M., Kvernmo, H.D.: Wavelet analysis of oscillations in the peripheral blood circulation measured by laser Doppler technique. IEEE Trans Biomed Eng. 46, 1230–1239 (1999). https://doi.org/10.1109/10.790500.
17. Tarantini, S., Tran, C.H.T., Gordon, G.R., Ungvari, Z., Csiszar, A.: Impaired neurovascular coupling in aging and Alzheimer's disease: contribution of astrocyte dysfunction and endothelial impairment to cognitive decline. Exp Gerontol. 94, 52–58 (2017). https://doi.org/10.1016/j.exger.2016.11.004.
18. Moore, C.I., Cao, R.: The Hemo-Neural Hypothesis: On The Role of Blood Flow in Information Processing. J Neurophysiol. 99, 2035–2047 (2008). https://doi.org/10.1152/jn.01366.2006.
19. Jindal, U., Sood, M., Dutta, A., Chowdhury, S.R.: Development of Point of Care Testing Device for Neurovascular Coupling From Simultaneous Recording of EEG and NIRS During Anodal Transcranial Direct Current Stimulation. IEEE J Transl Eng Health Med. 3, 2000112 (2015). https://doi.org/10.1109/JTEHM.2015.2389230.
20. Sancho, M., Samson, N.C., Hald, B.O., Hashad, A.M., Marrelli, S.P., Brett, S.E., Welsh, D.G.: KIR channels tune electrical communication in cerebral arteries. J Cereb Blood Flow Metab. 37, 2171–2184 (2017). https://doi.org/10.1177/0271678X16662041.
21. Fonteneau, C., Mondino, M., Arns, M., Baeken, C., Bikson, M., Brunoni, A.R., Burke, M.J., Neuvonen, T., Padberg, F., Pascual-Leone, A., Poulet, E., Ruffini, G., Santarnecchi, E., Sauvaget, A., Schellhorn, K., Suaud-Chagny, M.-F., Palm, U., Brunelin, J.: Sham tDCS: A hidden source of variability? Reflections for further blinded, controlled trials. Brain Stimul. 12, 668–673 (2019). https://doi.org/10.1016/j.brs.2018.12.977.
22. Tong, L., Hill, R.A., Damisah, E.C., Murray, K.N., Yuan, P., Bordey, A., Grutzendler, J.: Imaging and optogenetic modulation of vascular mural cells in the live brain. Nat Protoc. 16, 472–496 (2021). https://doi.org/10.1038/s41596-020-00425-w.